MORPHOMETRIC CHARACTERIZATION OF CRATER MODIFICATION IN DIVERSE SETTINGS ON MARS; W. A. Watters[1] (**wwatters@wellesley.edu**), C. I. Fassett,[2] C. Hundal,[1] R. Gibson[1]. [1]Dept. Astronomy, Whitin Observatory, Wellesley College; [2]Dept. Astronomy, Mount Holyoke College.

We examine the morphometry of simple impact craters measured from high-resolution topography created using stereo images from the HiRISE and CTX cameras on the Mars Reconnaissance Orbiter [1,2]. Our goal in this work is to quantitatively characterize the modification sequence of simple impact craters in diverse geological settings on Mars. This involves the use of rigorous statistical comparisons to identify distributions of morphometric parameter values that are characteristic of specific processes and conditions.

Previous work has addressed similar questions for larger impact craters on Mars using photoclinometric topography and laser altimetry [3,4,5]. More recently, HiRISE-derived topography and rover data have been used to characterize the modification of simple craters [e.g., 6,7,8,9]. A theoretical framework was long ago developed for understanding crater modification on the Moon [10], which has recently been examined using high-resolution topography [11,12].

Crater populations. We have assembled three catalogs of distinct impact crater populations and are working to expand these data sets by the time of the meeting. First is a globally-distributed population of 1,328 simple impact craters with diameter exceeding 500 m that occur in CTX stereo imagery and within $\pm 30^{o}$ latitude to avoid regions in which ice-related processes dominate the landscape evolution. All craters in this population derive from catalogs mapped by Robbins and Hynek [13,14].

Second, we examine 324 craters in the range 20 m < D < 800 m that occur in five HiRISE stereo pairs of the Meridiani hematite unit, including one that covers most of the Opportunity rover landing site [15]. The third population consists of 376 impact craters at the Spirit rover landing site, that occur dominantly in the Gusev floor plains surrounding the Columbia Hills: a densely-cratered region contained within a published HiRISE Science Team digital elevation model (DEM) [16]. The Meridiani and Gusev populations were selected for this study because the dominant surface materials and processes are relatively well-understood in light of results from the Mars Exploration Rover missions [6,7,8]. Many of the craters visited by these rovers are included in our database.

Data products. DEMs were generated for the global and Meridiani crater populations using the Ames Stereo Pipeline [17]. Image pairs were filtered to guarantee significant overlap and to ensure suitable illumination and viewing geometry to optimize DEM quality. In particular, we computed the parameters defined in [9] and used these to identify optimal stereo partners. All HiRISE stereo pairs used to generate the Meridiani DEMs were acquired as stereo observations in accordance with conventions prescribed by the HiRISE Science Team [2].

Shape extraction. A Hough circle transform was used to refine the locations of craters in cropped imagery and elevation models [18]. An automated process developed in-house and described in [9] was then used to trace the crater rim and extract radial topographic profiles. A minority of craters for which automatic techniques failed (e.g., failure to locate the crater or trace the rim accurately) have been discarded by manual inspection. In future work, these will be incorporated as our algorithm is refined, or else via manual and semi-automatic methods.

Morphometric parameters. We have computed morphometric parameters defined in [9] for all craters. These include traditional parameters such as rim height (h), rim-to-floor depth (d), and rim-to-rim diameter (D), in addition to measures of rim profile and planform shape, cavity and flank slopes, and cavity shape. Cavity shape is characterized by fitting a power law to radial cavity profiles. The exponent (α_c) is $\approx$1 for a conical cavities and $\approx$2 for paraboloidal cavities. Future work will make use of linear and nonlinear diffusion models to estimate parameters related to degradation state [12].

Measured distributions. Fig. 1 is a plot of d vs. D for all three populations, illustrating that the Gusev sample exhibits a much shallower d/D cut-off (roughly 0.07). Fig. 2 shows the diameter-normalized depth versus rim height for all three populations, illustrating a much tighter distribution in both parameters for the Gusev population, despite having more craters than the Meridiani sample. Fig. 3 compares the cumulative distribution functions for the cavity shape exponent (α_c) of all three populations. The two-sample KS test indicates an enormous difference between the Meridiani and Gusev cdfs for this quantity (p value $\ll$ 0.01).

Discussion. Surfaces on the Gusev plains are armored with a thin lag of relatively coarse grains [19]. The uppermost ~5-10 m are composed of a volcanic regolith; no bedrock exposures were encountered by the Spirit rover outside the Columbia Hills [6]. The Meridiani plains are underlain by a relatively soft evaporitic sandstone covered with < 1 m layer of mobile basaltic sands and a thin lag of coarse hematitic fragments [20]. At Meridiani, exposed (unarmored)

bedrock is quickly abraded and destroyed and cavities are sand-filled; these processes create a modification sequence that has been characterized using a combination of rover and orbiter imagery [6,7].

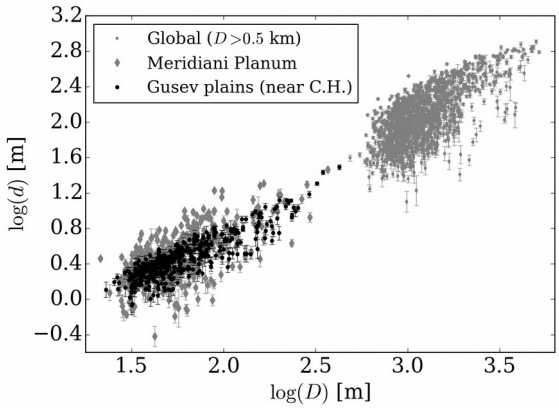

Fig. 1. Rim-to-floor depth (d) versus rim-to-rim diameter (D) for Meridiani Planum, the Gusev plains surrounding the Columbia Hills (C.H.), and a global sample of larger craters.

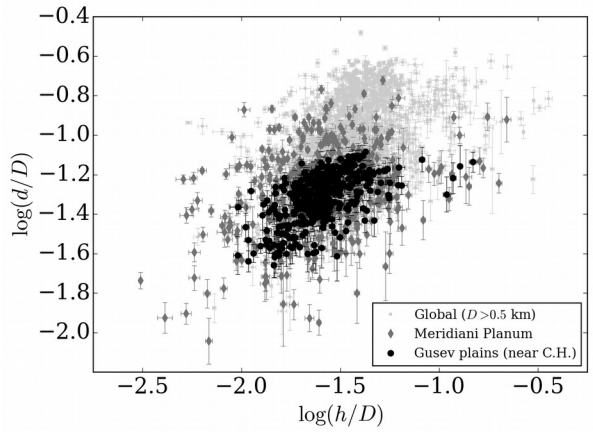

Fig. 2. Plot of diameter-normalized rim-to-floor depth versus crater rim height at Meridiani planum (gray circles) and the Gusev plains (black diamonds).

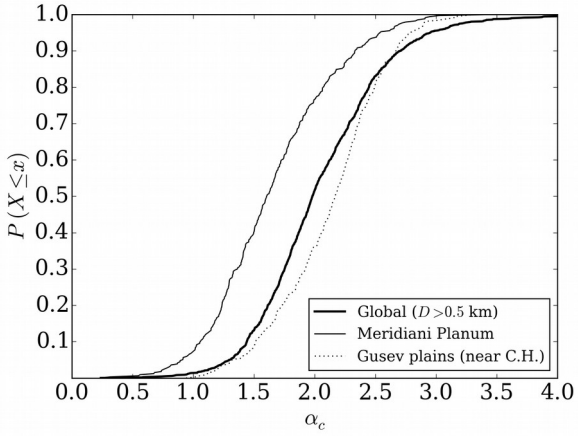

Fig. 3. Exponent of power-law fit to crater cavities (α_c). Meridiani Planum craters exhibit a relatively conical shape on average (α_c nearer to 1).

Our results indicate differences between the Gusev and Meridiani populations, although additional work is needed to establish their significance. Based on preliminary findings, we hypothesize that Meridiani craters tend to exhibit a more conical shape on account of the combined processes of episodic but efficient erosion and backwasting of crater rims mediated by sand abrasion and aeolian infilling of cavities [6]. By contrast, the more paraboloidal Gusev population may result from less efficient erosion versus relatively efficient infilling, which may be more typical of the martian surface in general at low latitudes.

An important challenge facing studies of this kind is to distinguish (a) the effects of variations in original crater shape caused by mechanical properties of target materials and the style of cratering, from (b) the variation that results from local, long-term degradation processes. The distinct trend and sharp cutoff in Fig. 1 for Gusev craters in d vs. D may imply that this population is dominated by secondaries, as previously concluded from rover observations [6]. Alternatively or in addition, the relatively tight bounds of the distribution of h/D and d/D may result from relatively restricted geographic sampling.

After expanding our database, future work will consist of detailed comparisons of the distributions of measured parameter values for a wide range of settings across Mars using rigorous statistical tests.

Acknowledgments. Work by Watters, Fassett, and Hundal was supported by a NASA Mars Data Analysis program grant (NNX15AM40G).

References: [1] Malin, M. et al. (2007) *JGR Planets*, *112*, ***E05S04;*** [2] McEwen, A. et al., (2007) *JGR*, *112*, E05S02; [3] Craddock, R. A., et al. (1997) *JGR Planets*, *102*, *13321–13340;* [4] Garvin, J. et al.(2000), *Icarus*, *144*, 329-352; [5] Whitehead, J., et al. (2010) *GSA special papers*, *465*, 67-81; [6] Grant et al. (2006) *JGR Planets*, *111*, E02S08; [7] Grant et al. (2008) *JGR Planets*, *113*, E11010; [8] Golombek, M. et al. (2014) *JGR Planets*, *119*, *2522–2547;* [9] Watters, W.A. et al., (2015) *JGR Planets*, doi: 10.1002/2014JE004630; [10] Soderblom, L.A., & Lebofsky, L.A., (1972) *JGR*, 77, *279–296;* [11] Basilevsky et al. (2014) *PSS*, *92*, *77-87;* [12] Fassett, C.I., & B.J. Thomson (2014) *JGR Planets*, *119*, *2255-2271;* [13] Robbins S. & Hynek B. (2012) *JGR-Planets*, *117*, E05004; [14] Robbins S., *personal comm.;* [15] ESP_021747_1780 & ESP_022380_1780; [16] DTEEC_001513_1655_ 001777_1650; [17] Moratto, Z., et al., (2010) *LPSC 41*, #2364; [18] Bue, B..D. & Stepinski, T.F. (2007) *IEEE Trans. Geosci. & Remote Sensing*, *45*, *265-274;* [19] Greeley et al. (2004) *Science*, *305; 810,819-821;* [20] Soderblom, L.A., & Lebofsky, L.A., (1972) *JGR*, 77, *279–296*